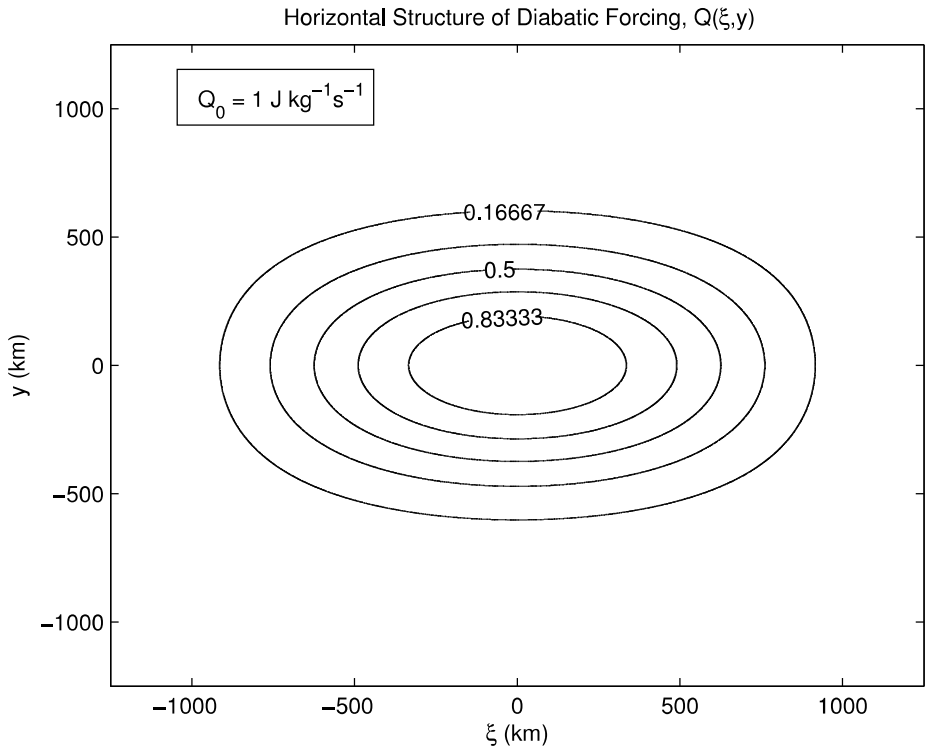

Figure 2.2: Contour plot of the diabatic forcing horizontal structure with Q_0 set to 1 J $\mathrm{kg}^{-1}\mathrm{s}^{-1}$.

of (2.15) yields $\iint \hat{Q}(\xi, y)\, dxdy = \pi^{\frac{1}{2}} Q_0 a_0 b_0$, so that our variation of the parameter y_0 has no effect on the total diabatic heating rate, $\pi^{\frac{1}{2}} Q_0 a_0 b_0$.

2.4 Horizontal Structure Problem

Our interest is in observing the flow field around the eastward moving constant source once all transient effects have ended. If we assume that it does reach a steady state, then viewing it from a reference frame that is moving at the same speed as the source would allow us to study the unchanging response pattern, versus watching the evolution of a particular region as the source passes through it. From this vantage point a change in time is proportional to a change in zonal position of the earth-relative steady state circulation. The shallow water equations (2.14) are converted to a system that is valid in this moving frame of reference by transforming both time and zonal derivatives to derivatives of the

"translating zonal distance coordinate" (ξ), introduced in the previous section. Making the replacements (see Appendix C for justification)

$$\frac{\partial}{\partial x} = \frac{\partial}{\partial \xi}, \tag{2.16}$$

$$\frac{\partial}{\partial t} = -c\frac{\partial}{\partial \xi}, \tag{2.17}$$

in (2.14) results in

$$\begin{aligned} -c\frac{\partial \hat{u}}{\partial \xi} - \beta y\hat{v} + \frac{\partial \hat{\phi}}{\partial \xi} &= -\alpha\hat{u}, \\ -c\frac{\partial \hat{v}}{\partial \xi} + \beta y\hat{u} + \frac{\partial \hat{\phi}}{\partial y} &= -\alpha\hat{v}, \\ \hat{\phi} &= R\hat{T}, \\ \frac{\partial \hat{u}}{\partial \xi} + \frac{\partial \hat{v}}{\partial y} - \left(\frac{\pi^2}{z_T^2} + \frac{1}{4}\right)\hat{w} &= 0, \\ -c\frac{\partial \hat{T}}{\partial \xi} + \Gamma\hat{w} &= -\alpha\hat{T} + \frac{\hat{Q}}{c_p}, \end{aligned} \tag{2.18}$$

reducing the number of independent variables from three to two. Next take the Fourier ξ-transform of the resulting system, defining, for example,

$$\hat{u}_m(y) = \frac{1}{2\pi a}\int_{-\pi a}^{\pi a} \hat{u}(\xi, y)e^{-im\xi/a}d\xi, \quad \hat{u}(\xi, y) = \sum_{m=-\infty}^{\infty} \hat{u}_m(y)e^{im\xi/a}, \tag{2.19}$$

where the integer m denotes the zonal wavenumber. Similar Fourier transform pairs exist for $\hat{v}_m(y)$, $\hat{\phi}_m(y)$, $\hat{T}_m(y)$, $\hat{w}_m(y)$, and $\hat{Q}_m(y)$. In this way, system (2.18) reduces to

$$\begin{aligned} \left(\alpha - \frac{imc}{a}\right)\hat{u}_m - \beta y\hat{v}_m + \frac{im}{a}\hat{\phi}_m &= 0, \\ \left(\alpha - \frac{imc}{a}\right)\hat{v}_m + \beta y\hat{u}_m + \frac{d\hat{\phi}_m}{dy} &= 0, \\ \left(\alpha - \frac{imc}{a}\right)\hat{\phi}_m + \bar{c}^2\left(\frac{im}{a}\hat{u}_m + \frac{d\hat{v}_m}{dy}\right) &= \kappa\hat{Q}_m, \end{aligned} \tag{2.20}$$

after eliminating $\hat{w}_m$ and $\hat{T}_m$ by combining the hydrostatic, continuity, and thermodynamic equations. For each integer wavenumber m, (2.20) is a system of equations dependent only on meridional position. Once (2.20) has been solved for $\hat{u}_m$, $\hat{v}_m$, $\hat{\phi}_m$, the vertical velocity $\hat{w}_m$ can be recovered from

$$\hat{w}_m = \left(\frac{\pi^2}{z_T^2} + \frac{1}{4}\right)^{-1}\left(\frac{im}{a}\hat{u}_m + \frac{d\hat{v}_m}{dy}\right). \tag{2.21}$$

The Fourier ξ-transform of $\hat{Q}(\xi, y)$, defined by (2.15), is given by

$$\hat{Q}_m(y) = (2\pi a)^{-1} \int_{-\pi a}^{\pi a} \hat{Q}(\xi, y) \exp(-im\xi/a) d\xi,$$

which is easily evaluated to yield

$$\hat{Q}_m(y) = \frac{\pi Q_0}{2[\pi^2 - (ma_0/a)^2]} \frac{\sin(ma_0/a)}{m} \exp\left[- \left(\frac{y - y_0}{b_0} \right)^2 \right]. \tag{2.22}$$

We now write the system (2.20) in the convenient vector form [1]

$$\left(\alpha - \frac{imc}{a} \right) \hat{\boldsymbol{\eta}}_m + \mathcal{L} \hat{\boldsymbol{\eta}}_m = \kappa \hat{\mathbf{Q}}_m, \tag{2.23}$$

where

$$\mathcal{L} = \begin{pmatrix} 0 & -\beta y & im/a \\ \beta y & 0 & d/dy \\ \bar{c}^2 im/a & \bar{c}^2 d/dy & 0 \end{pmatrix}, \quad \hat{\boldsymbol{\eta}}_m(y) = \begin{pmatrix} \hat{u}_m(y) \\ \hat{v}_m(y) \\ \hat{\phi}_m(y) \end{pmatrix}, \quad \hat{\mathbf{Q}}_m(y) = \begin{pmatrix} 0 \\ 0 \\ \hat{Q}_m(y) \end{pmatrix}. \tag{2.24}$$

The Fourier transformed equations (2.23) can be solved using a normal mode transform in the meridional direction. To accomplish this, first define the inner product

$$(\mathbf{f}, \mathbf{g}) = \int_{-\infty}^{\infty} \left(f_1 g_1^* + f_2 g_2^* + \frac{1}{\bar{c}^2} f_3 g_3^* \right) d\hat{y}, \tag{2.25}$$

where $\mathbf{f}(\hat{y})$ and $\mathbf{g}(\hat{y})$ are complex, three component vector functions of the dimensionless meridional coordinate $\hat{y} = (\beta/\bar{c})^{\frac{1}{2}} y = \epsilon^{\frac{1}{4}} (y/a)$, and where the * symbol denotes the complex conjugate and $\epsilon = 4\Omega^2 a^2/\bar{c}^2$ is Lamb's parameter. With $\bar{c} = 41.25$ m s^{-1} we obtain $\epsilon = 507.3$. The inner product (2.25), is suggested by the total energy principle (derived in section 4.1) associated with (2.23). The adjoint of $\mathcal{L}$, denoted by $\mathcal{L}^\dagger$ and defined by $(\mathcal{L}\mathbf{f}, \mathbf{g}) = (\mathbf{f}, \mathcal{L}^\dagger \mathbf{g})$, is related to $\mathcal{L}$ by $\mathcal{L}^\dagger = -\mathcal{L}$. In other words, the linear operator $\mathcal{L}$ is skew-Hermitian with respect to the inner product (2.25). The skew-Hermitian property dictates that the eigenvalues of $\mathcal{L}$ are pure imaginary and that the eigenfunctions form a complete

[1] The simplicity of the first term in (2.23) depends on the assumed equality for the damping rates associated with Rayleigh friction and Newtonian cooling. However, the derivation following (2.23) could easily be generalized to allow a 10–20 day radiative damping rate and a 3–5 day frictional damping rate (Lin et al., 2005).

(Wu and Moore, 2004), orthogonal set (as long as degeneracy does not occur). Denoting an eigenvalue by $i\nu_{mnr}$ and a corresponding eigenfunction by $\mathbf{K}_{mnr}(\hat{y})$, we have

$$\mathcal{L}\mathbf{K}_{mnr} = i\nu_{mnr}\mathbf{K}_{mnr}, \quad \text{with} \quad \mathbf{K}_{mnr}(\hat{y}) = \begin{pmatrix} U_{mnr}(\hat{y}) \\ V_{mnr}(\hat{y}) \\ \Phi_{mnr}(\hat{y}) \end{pmatrix}. \tag{2.26}$$

The eigenvalues of $\mathcal{L}$, which yield the dispersion relation for equatorially trapped waves,

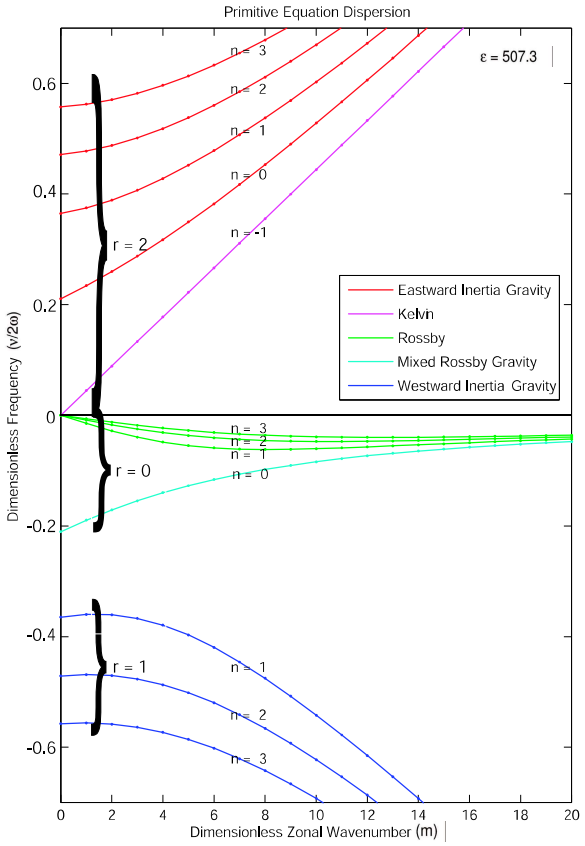

Figure 2.3: Dispersion diagram, $\hat{\nu}_{mnr}$ vs. m, for values $n = -1, 0, 1, 2, 3$ and $r = 0, 1, 2$.

satisfy the cubic equation (Matsuno, 1966)

$$\epsilon\hat{\nu}^2 - m^2 - \frac{m}{\hat{\nu}} = \epsilon^{\frac{1}{2}}(2n+1), \tag{2.27}$$

where $n = 0, 1, 2, \cdots$ is the index for the meridional mode and $\hat{\nu} = \nu/(2\Omega)$ is the dimensionless frequency. We let $r = 0, 1, 2$ be the index corresponding to the three roots of the

dispersion relation, so that the eigenfunctions and eigenvalues can be characterized by the triple index m, n, r. Special care is required for the case $n = 0$, for which (2.27) can be factored into $(\epsilon^{\frac{1}{2}}\hat{\nu} + m)(\epsilon^{\frac{1}{2}}\hat{\nu}^2 - m\hat{\nu} - 1) = 0$. The root $\epsilon^{\frac{1}{2}}\hat{\nu} = -m$ must be discarded because the corresponding eigenfunction is unbounded in $\hat{y}$. Thus, when $n = 0$, only the two solutions of $\epsilon^{\frac{1}{2}}\hat{\nu}^2 - m\hat{\nu} - 1 = 0$ are retained and are indexed by $r = 0$ (mixed Rossby-gravity wave) and $r = 2$ (eastward inertia-gravity wave). The eigenfunctions for Kelvin waves can be found separately by setting V_{mnr} to zero in (2.26). The Kelvin wave eigenvalues $\epsilon^{\frac{1}{2}}\hat{\nu} = m$ can be formally considered as a solution to (2.27) when $n = -1$. We index this solution as $r = 2$. Then, for given $n = -1, 0, 1, \cdots$, $\mathbf{K}_{mnr}(\hat{y})$ is the eigenfunction corresponding to the eigenvalue ν_{mnr}. The form of $\mathbf{K}_{mnr}(\hat{y})$ is given by

$$\mathbf{K}_{mnr}(\hat{y}) = A_{mnr} \begin{pmatrix} \epsilon^{\frac{1}{4}} \left[\left(\epsilon^{\frac{1}{2}}\hat{\nu}_{mnr} + m \right) \left(\frac{n+1}{2} \right)^{\frac{1}{2}} \mathcal{H}_{n+1}(\hat{y}) + \left(\epsilon^{\frac{1}{2}}\hat{\nu}_{mnr} - m \right) \left(\frac{n}{2} \right)^{\frac{1}{2}} \mathcal{H}_{n-1}(\hat{y}) \right] \\ -i \left(\epsilon \hat{\nu}_{mnr}^2 - m^2 \right) \mathcal{H}_n(\hat{y}) \\ \overline{c}\epsilon^{\frac{1}{4}} \left[\left(\epsilon^{\frac{1}{2}}\hat{\nu}_{mnr} + m \right) \left(\frac{n+1}{2} \right)^{\frac{1}{2}} \mathcal{H}_{n+1}(\hat{y}) - \left(\epsilon^{\frac{1}{2}}\hat{\nu}_{mnr} - m \right) \left(\frac{n}{2} \right)^{\frac{1}{2}} \mathcal{H}_{n-1}(\hat{y}) \right] \end{pmatrix}, \tag{2.28}$$

where the meridional structure functions $\mathcal{H}_n(\hat{y})$ $(n = 0, 1, 2, \ldots)$ are related to the Hermite polynomials $H_n(\hat{y})$ $(n = 0, 1, 2, \ldots)$ by [2]

$$\mathcal{H}_n(\hat{y}) = \left(\pi^{\frac{1}{2}} 2^n n! \right)^{-\frac{1}{2}} H_n(\hat{y}) e^{-\frac{1}{2}\hat{y}^2}. \tag{2.29}$$

Since the Hermite polynomials satisfy the recurrence relation $\hat{y}H_n(\hat{y}) = \frac{1}{2}H_{n+1}(\hat{y}) + nH_{n-1}(\hat{y})$ and the derivative relation $dH_n(\hat{y})/d\hat{y} = 2nH_{n-1}(\hat{y})$, it is easily shown that the meridional structure functions $\mathcal{H}_n(\hat{y})$ satisfy the recurrence relation

$$\hat{y}\mathcal{H}_n(\hat{y}) = \left(\frac{n+1}{2} \right)^{\frac{1}{2}} \mathcal{H}_{n+1}(\hat{y}) + \left(\frac{n}{2} \right)^{\frac{1}{2}} \mathcal{H}_{n-1}(\hat{y}), \tag{2.30}$$

and the derivative relation

$$\frac{d\mathcal{H}_n(\hat{y})}{d\hat{y}} = -\left(\frac{n+1}{2} \right)^{\frac{1}{2}} \mathcal{H}_{n+1}(\hat{y}) + \left(\frac{n}{2} \right)^{\frac{1}{2}} \mathcal{H}_{n-1}(\hat{y}). \tag{2.31}$$

[2] The meridional structure functions $\mathcal{H}_n$ are more convenient for our purposes than the parabolic cylinder functions D_n. The two functions are related by $\mathcal{H}_n(\hat{y}) = (\pi^{\frac{1}{2}} n!)^{-\frac{1}{2}} D_n(2^{\frac{1}{2}}\hat{y})$.

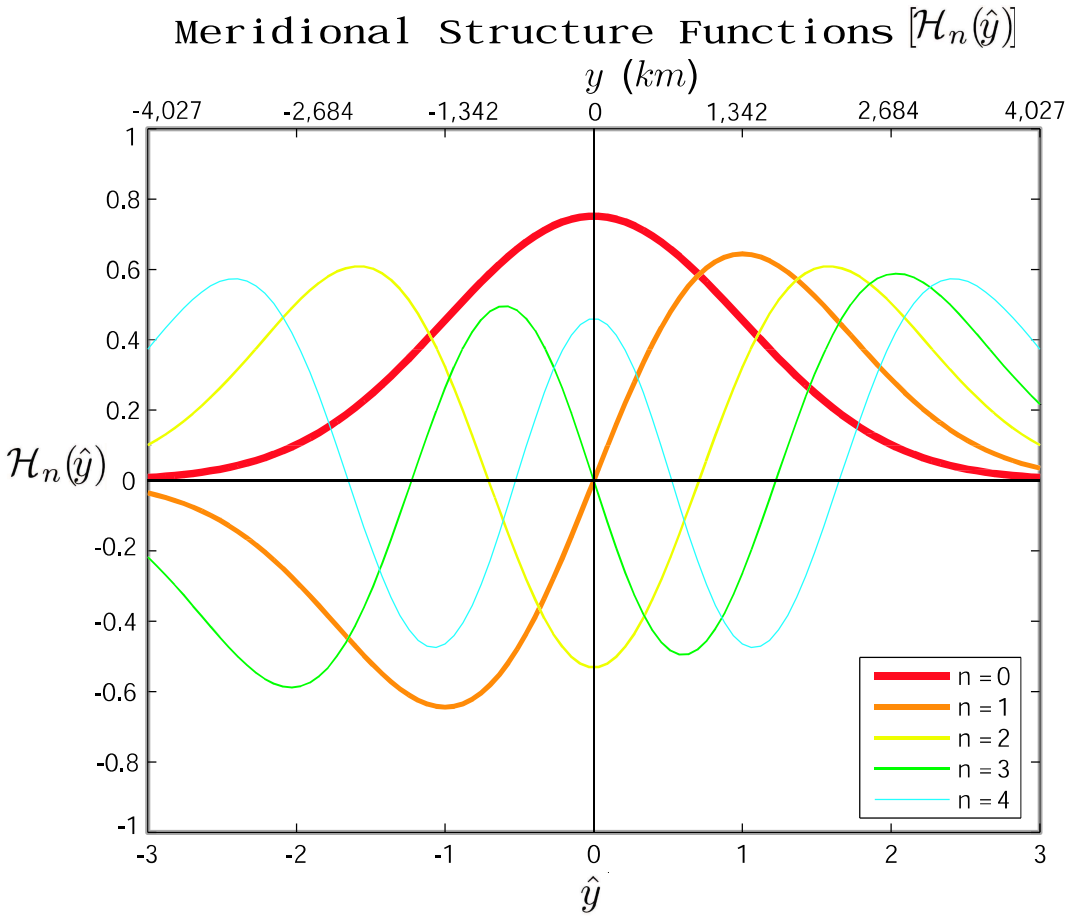

Figure 2.4: The meridional structure functions, $\mathcal{H}_n(\hat{y})$ for $n = 0, 1, 2, 3, 4$, are plotted over the equatorial band $\sim$ (35°S, 35°N). The lower axis displays dimensionless meridional distance, $\hat{y} = \epsilon^{\frac{1}{4}}(y/a)$, and the upper axis displays the corresponding (integer) dimensional meridional distance, y km.

The first two meridional structure functions are $\mathcal{H}_0(\hat{y}) = \pi^{-\frac{1}{4}} e^{-\frac{1}{2}\hat{y}^2}$ and $\mathcal{H}_1(\hat{y}) = 2^{\frac{1}{2}}\pi^{-\frac{1}{4}}\hat{y}e^{-\frac{1}{2}\hat{y}^2}$, from which all succeeding structure functions can be computed using the recurrence relation (2.30). Computing $\mathcal{H}_n(\hat{y})$ via its recurrence relation is much preferable to computing $H_n(\hat{y})$ via its recurrence relation and then computing $\mathcal{H}_n(\hat{y})$ by evaluation of the right hand side of (2.29), because the former method avoids explicit calculation of the factor $2^n n!$ for large n. Plots of $\mathcal{H}_n(\hat{y})$ for $n = 0, 1, 2, 3, 4$ are shown in Fig. 2.4. The normalization factor in (2.28) is given by

$$A_{mnr} = \left[\epsilon^{\frac{1}{2}}(n+1)\left(\epsilon^{\frac{1}{2}}\hat{\nu}_{mnr} + m\right)^2 + \epsilon^{\frac{1}{2}} n\left(\epsilon^{\frac{1}{2}}\hat{\nu}_{mnr} - m\right)^2 + \left(\epsilon\hat{\nu}_{mnr}^2 - m^2\right)^2\right]^{-\frac{1}{2}} \qquad (2.32)$$

for $n \geq 0$ and by

$$A_{m,-1,2} = 2^{-\frac{1}{2}}\pi^{-\frac{1}{4}} \tag{2.33}$$

for $n = -1$. These normalization factors result in the orthonormality property

$$\left(\mathbf{K}_{mnr}(\hat{y}), \mathbf{K}_{mn'r'}(\hat{y})\right) = \begin{cases} 1 & (n', r') = (n, r) \\ 0 & (n', r') \neq (n, r). \end{cases} \tag{2.34}$$

The normality part of (2.34) is easily confirmed by substituting (2.28) into the left hand side and then using

$$\int_{-\infty}^{\infty} \mathcal{H}_n(\hat{y})\mathcal{H}_{n'}(\hat{y})d\hat{y} = \begin{cases} 1 & n' = n, \\ 0 & n' \neq n \end{cases} \tag{2.35}$$

to evaluate the three resulting integrals. It should be noted that there is a degeneracy for the zonally symmetric Rossby modes (i.e., for $m = 0$, $n > 0$, $r = 0$), in which case (2.28) is indeterminant because both m and $\hat{\nu}_{0n0}$ vanish. However, orthonormal eigenfunctions are easily constructed in this case, as discussed in Appendix D. Because of the orthonormality and completeness of the eigenfunctions $\mathbf{K}_{mnr}(\hat{y})$, we can set up the transform pair (Silva Dias et al., 1983; DeMaria, 1985)

$$\hat{\eta}_{mnr} = \left(\hat{\boldsymbol{\eta}}_m(\hat{y}), \mathbf{K}_{mnr}(\hat{y})\right), \tag{2.36}$$

$$\hat{\boldsymbol{\eta}}_m(\hat{y}) = \sum_{n=-1}^{\infty} \sum_{r} \hat{\eta}_{mnr}\mathbf{K}_{mnr}(\hat{y}), \tag{2.37}$$

where $\hat{\eta}_{mnr}$ are the scalar coefficients in the normal mode expansion of the vector $\hat{\boldsymbol{\eta}}_m(\hat{y})$. Note that (2.36) can be obtained by taking the inner product of (2.37) with $\mathbf{K}_{mn'r'}(\hat{y})$ and using the orthonormality property (2.34).

We now have the tools necessary to solve (2.23). Start by taking the inner product of (2.23) with the eigenfunction $\mathbf{K}_{mnr}(\hat{y})$,

$$\left(\left(\alpha - \frac{imc}{a}\right)\hat{\boldsymbol{\eta}}_m, \mathbf{K}_{mnr}(\hat{y})\right) + (\mathcal{L}\hat{\boldsymbol{\eta}}_m, \mathbf{K}_{mnr}(\hat{y})) = \left(\kappa\hat{\mathbf{Q}}_m, \mathbf{K}_{mnr}(\hat{y})\right),$$

next use the Skew-Hermitian property of $\mathcal{L}$,

$$\left(\alpha - \frac{imc}{a}\right)(\hat{\boldsymbol{\eta}}_m, \mathbf{K}_{mnr}(\hat{y})) + (\hat{\boldsymbol{\eta}}_m, -\mathcal{L}\mathbf{K}_{mnr}(\hat{y})) = \kappa\left(\hat{\mathbf{Q}}_m, \mathbf{K}_{mnr}(\hat{y})\right),$$

use the eigen-relation (2.26), (2.36), and the inner product $\hat{Q}_{mnr} = (\hat{\mathbf{Q}}_m, \mathbf{K}_{mnr})$,

$$\left(\alpha - \frac{imc}{a}\right)\hat{\eta}_{mnr} + i\nu_{mnr}\left(\hat{\boldsymbol{\eta}}_m, \mathbf{K}_{mnr}(\hat{y})\right) = \kappa\hat{Q}_{mnr},$$

finally,

$$\hat{\eta}_{mnr} = \frac{\kappa\hat{Q}_{mnr}}{\alpha + i(\nu_{mnr} - cm/a)}. \tag{2.38}$$

We have reduced the set of ordinary differential equations (2.23), to a decoupled system of algebraic equations (2.38), which can be solved independently for the values of $\hat{\eta}_{mnr}$. An expression for $(\hat{\mathbf{Q}}_m, \mathbf{K}_{mnr})$ is derived using the integral given in Appendix E. Using the result (E.1) twice, once with n replaced by $n+1$ and once with n replaced by $n-1$, we can write $\hat{Q}_{mnr}$ as

$$\begin{aligned}\hat{Q}_{mnr} =& \frac{A_{mnr}\epsilon^{\frac{1}{2}}\pi Q_0 a_0 b_0}{2\bar{c}a^2[\pi^2 - (ma_0/a)^2]}\frac{\sin(ma_0/a)}{(ma_0/a)}\left(\frac{2\pi}{2+\hat{b}_0^2}\right)^{\frac{1}{2}}\exp\left(\frac{\hat{b}_0^2\hat{y}_0^2}{4-\hat{b}_0^4}\right)\\ &\cdot\left[(\epsilon^{\frac{1}{2}}\hat{\nu}_{mnr} + m)\left(\frac{2-\hat{b}_0^2}{2+\hat{b}_0^2}\right)^{\frac{n+1}{2}}\left(\frac{n+1}{2}\right)^{\frac{1}{2}}\mathcal{H}_{n+1}\left(\frac{2\hat{y}_0}{(4-\hat{b}_0^4)^{\frac{1}{2}}}\right)\right.\\ &\left.-(\epsilon^{\frac{1}{2}}\hat{\nu}_{mnr} - m)\left(\frac{2-\hat{b}_0^2}{2+\hat{b}_0^2}\right)^{\frac{n-1}{2}}\left(\frac{n}{2}\right)^{\frac{1}{2}}\mathcal{H}_{n-1}\left(\frac{2\hat{y}_0}{(4-\hat{b}_0^4)^{\frac{1}{2}}}\right)\right]\end{aligned} \tag{2.39}$$

for $n \geq 0$, and as

$$\hat{Q}_{mnr} = \frac{A_{mnr}\epsilon^{\frac{1}{4}}\pi Q_0 a_0 b_0}{2\bar{c}a^2[\pi^2 - (ma_0/a)^2]}\frac{\sin(ma_0/a)}{(ma_0/a)}\left(\frac{2\pi}{2+\hat{b}_0^2}\right)^{\frac{1}{2}}\exp\left(-\frac{\hat{y}_0^2}{2+\hat{b}_0^2}\right). \tag{2.40}$$

for the Kelvin wave ($n = -1$, $r = 2$).

After $\hat{\eta}_{mnr}$ is computed from (2.38)–(2.40), the physical space fields u, v, ϕ can be recovered by making use of (2.37), followed by the inverse Fourier transform in ξ, i.e.,

$$\begin{pmatrix} u(\xi,y,z) \\ v(\xi,y,z) \\ \phi(\xi,y,z)\end{pmatrix} = Z(z)\sum_{m=-\infty}^{\infty}\sum_{n=-1}^{\infty}\sum_{r}\hat{\eta}_{mnr}\begin{pmatrix} U_{mnr}(\hat{y}) \\ V_{mnr}(\hat{y}) \\ \Phi_{mnr}(\hat{y})\end{pmatrix}e^{im\xi/a}. \tag{2.41}$$

Using (2.21), (2.28) and (2.31) the physical space vertical log-pressure velocity can be recovered from

$$w(\xi,y,z) = \frac{Z'(z)}{R\Gamma}\sum_{m=-\infty}^{\infty}\sum_{n=-1}^{\infty}\sum_{r} i\nu_{mnr}\hat{\eta}_{mnr}\Phi_{mnr}(\hat{y})e^{im\xi/a}. \tag{2.42}$$

For later use we note that the vertical log-pressure velocity $w = Dz/Dt$ is related to the vertical p-velocity $\omega = Dp/Dt$ by $\omega = -p_0 e^{-z} w$.

2.5 Solutions

All the model results shown in this section have been constructed by numerical evaluation of (2.41), and (2.42), which involves a superposition of zonal wavenumbers (sum over m), meridional wavenumbers (sum over n), and wave types (sum over r). In our examples the spectral coefficients $\hat{\eta}_{mnr}$ decay exponentially with n for all choices of m, which enables us to truncate the spectral solution at $n = N$ with a specified degree of accuracy. In general, $N = 200$ gives accurate results. Appendix F displays a flow chart outlining the procedure for computing the solutions.

Although the solutions have been computed over the entire zonal domain, only half the domain, centered on the forcing, is shown. This allows greater detail to be displayed for the region nearest the forcing. Using the parameters listed in Table 2.1, the 850 hPa wind and geopotential fields computed from (2.41) are shown in the top panel of Fig. 2.5 for $y_0 = 0$ and in the top panel of Fig. 2.7 for $y_0 = 450$ km. The choice of 850 hPa as the display level is arbitrary. According to the profile of $Z(z)$ shown in Fig. 2.1, upper tropospheric fields have the opposite sign and approximately twice the magnitude of the lower tropospheric fields. An interesting property of these simple linear solutions is that the lower tropospheric maximum westerly winds in the wake of the convective envelope are stronger than the lower tropospheric maximum easterly winds ahead of the convection. For example, in Fig. 2.5 the maximum 850 hPa westerly flow is 3.7 $\mathrm{m\,s^{-1}}$ while the maximum easterly flow is 1.6 $\mathrm{m\,s^{-1}}$. In Fig. 2.7 the corresponding values are 4.2 $\mathrm{m\,s^{-1}}$ and 1.4 $\mathrm{m\,s^{-1}}$. These wind speeds, the degree of asymmetry between westerlies and easterlies, and the larger zonal extent of the easterlies compared to the westerlies all agree well with the observed MJO composite [3]

[3] There is substantial variability in the cases that make up the MJO composite so that a detailed comparison of model results with an individual MJO case probably requires modeling the details of the diabatic forcing associated with that case.